Radio Science, Volume 6, Number 1, pages 65–86, January 1971

Study of magnetospheric field oriented irregularities—the mode theory of bell-shaped ducts

R. R. Scarabucci[1] *and R. L. Smith*

Radioscience Laboratory, Stanford University
Stanford, California 94305

(Received November 24, 1969; revised August 17, 1970.)

The propagation of whistler energy in slight enhancements or depressions of ionization aligned with the geomagnetic field has been studied earlier in the two limiting cases of a discontinuous boundary or very slowly varying density gradients. These two approaches have yielded different results, particularly for the trapping of energy in enhancements of ionization. Therefore a study of the reflection and transmission for the full range of gradients is desirable. In this paper, full-wave methods are applied to bell shaped ducts of arbitrary scale size. The results indicate criteria for applicability of the two simplifying limiting cases. This phase of the study is further extended by examination of a coupling theory. For a variety of magnetospheric conditions the cross-coupling terms between characteristically different waves are negligible; this leads to almost perfect reflection and substantiates the use of the simpler phase-integral techniques. By using the phase integral techniques, we have derived a fairly complete description of possible modes excited in bell shaped ducts. For each mode a theoretical whistler spectrogram is obtained. Extensions of the theory to apply to nonuniform magnetic fields may lead to predictions of a hyper-fine whistler structure.

1. INTRODUCTION

This paper deals with the propagation of whistler waves along field oriented irregularities, or ducts of enhanced ionization. Theoretical studies that begin with a simple step-discontinuity model have indicated that a duct of enhanced ionization is 'leaky' and that a significant amount of energy will be lost to non-trapped modes. Such leakages do not appear in the simpler theories where WKB methods are assumed valid. One suspects then that any leakage from the duct should be related to the magnitude of the gradients of electron density across the duct. In this paper the loss factors as a function of irregularity scale-size are studied by using a full-wave technique. One of the interesting results is that the leakage may be quite small even for irregularities with scale sizes much smaller than characteristic wavelengths of the trapped modes.

2. BRIEF OUTLINE OF THE EARLIER WORK

In his classic paper, *Storey* [1953] showed that if the frequencies of the whistler components were much smaller than both the electron gyrofrequency and the plasma frequency along the whistler path, then the whistler packet should travel approximately along the earth's magnetic field. Under the above circumstances the maximum departure of the rays relative to the field lines would be 19°29′. Storey also observed long trains of echoes from whistlers in which the amplitude decayed very slowly through the train. He suggested that ionospheric irregularities like columns of auroral ionization could have a guiding effect on the waves and thus would explain the low amplitude decrement. This idea was extended by *Helliwell et al.* [1956] to explain the discrete traces often exhibited in the spectrograms of whistlers. It was suggested that each trace resulted from the concentration of energy in a thin column of ionization acting as a duct and extending over a large part of the ray trajectory in the magnetosphere [*Helliwell*, 1956]. A first ray theory of whistler propagation that is supported by field oriented irregularities of electron density (ducts) was presented by *Smith et al.* [1960]. They showed that trapping was possible in both enhancements and depressions of ionization. *Smith* [1961] concluded that whistlers propagate in ducts of enhanced ionization and that for such propagation there exists a cutoff frequency at ap-

[1] Now at Comissaõ Nacional de Atividades Espaciais, São José dos Campos, São Paulo, Brazil.

proximately one-half the minimum gyrofrequency along the whistler path. *Voge* [1961, 1962] calculated the minimum change in ionization and the corresponding minimum width of the ducts that are required for the trapping by using a method developed for tropospheric ducts. Similar calculations were presented by *Booker* [1962], who assumed purely longitudinal propagation along the geomagnetic field lines of a model magnetosphere, The Booker paper has been extended by *Walker* [1966*b*, *c*], who took into account the anisotropy of the medium. *Walker* [1966*a*] also made the first application of a full-wave technique to analyze the propagation of a locally plane wave based on the phase integral formula. *Adachi* [1965] studied the trapping of waves in very narrow sharply bounded slabs of ionization oriented along the magnetic field of a homogeneous magnetoionic medium. He concluded that, for whistler frequencies below one-half the gyrofrequency, only partially trapped (leaky) waves could propagate along the slab of enhanced ionization.

Gothard [1968] presented a mode theory for the guidance of waves along an inhomogeneous field-aligned plasma stratum by using the phase integral method. In his model the guiding structure is a bell shaped duct. He assumed that the profile across the duct varied slowly enough to permit no leakage.

3. THE PRESENT WORK

In this paper a full-wave technique described in section 4 will be applied to propagation through planar field-oriented irregularities. In this case it is possible to simplify some equations of the complete full-wave analysis, and a simpler computer program can be used to obtain the behavior of the electromagnetic fields (section 5).

In section 6 we will develop the mode theory of homogeneous field-oriented ducts whose transverse section has a bell shaped variation of electron density. The full-wave treatment is locally applied for a plane wave in the magnetosphere where the electron profile presents a bell shaped enhancement and the effect of heavy ions is ignored. However, the full-wave method is able to handle any symmetric field-oriented duct in which electron and ion densities are allowed to vary arbitrarily. Under certain conditions the numerical full-wave method permits the use of a phase-integral method which may then profitably replace the more lengthy full-wave technique.

Although the mode theory of bell shaped ducts is the ultimate result of this paper, the more important results (from the standpoint of wave-propagation theory) are derived in section 5, in which the waves excited at field-oriented irregularities are studied. In section 5 the results of the numerical full-wave technique are compared with the coupling theory of *Budden and Clemmow* [1957]. This comparison is fruitful and leads to a simple interpretation of the reflection phenomenon.

4. FULL-WAVE TREATMENT OF WAVE PROPAGATION THROUGH PLANAR IRREGULARITIES OF A MAGNETOIONIC MEDIUM

Suppose there is a characteristic electromagnetic plane wave propagating in a homogeneous ionosphere and that the wave is incident upon a planarly stratified irregularity. The geometry is such that the planes of stratification are parallel to the (xy) plane (see Figure 1). The (yz) plane contains the earth's magnetic field, which makes an angle *DIP* with the y axis. The wave normal of the incident wave makes an angle I with the z axis (angle of incidence) and an angle χ with the magnetic meridian (azimuthal angle). It is also assumed that between two heights z_0 and z_1 the medium parameters vary arbitrarily, but for $z \leq z_0$ and $z \geq z_1$ the medium is homogeneous. One example is shown in Figure 2, where the electron density is taken as the variable parameter of the medium.

The problem is to determine the reflected and the

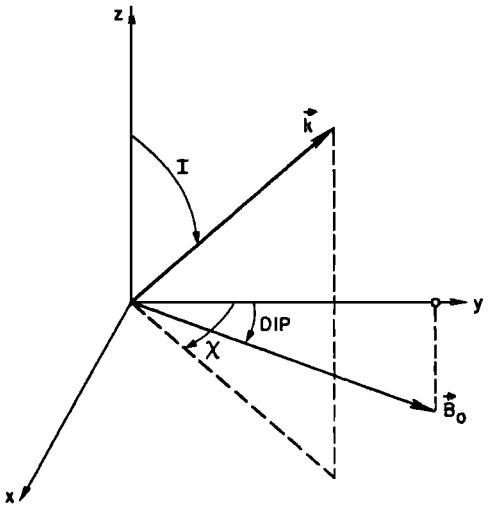

Fig. 1. The coordinate system and the incident vector k. The direction of k is defined by the incident angle I and the azimuthal angle χ. The magnetic field B_0 is in the (yz) plane.

transmitted waves for $z < z_0$ and $z > z_1$, respectively. Since it is assumed from the outset that the medium is not slowly varying, it is necessary to develop a numerical full-wave technique for solving the problem. The full-wave treatment followed in this paper is briefly described below.

Beginning with Maxwell's equations and assuming a planarly stratified medium, *Clemmow and Heading* [1954] derived the following set of differential equations governing the propagation of plane waves inside the medium:

$$d\mathbf{e}/dz = -jk\tilde{T}\cdot\mathbf{e} \tag{1}$$

where $\mathbf{e}$ is the column vector

$$\mathbf{e} = \begin{bmatrix} E_x \\ -E_y \\ Z_0H_x \\ Z_0H_y \end{bmatrix} \tag{2}$$

The symbols $\mathbf{E} = (E_x, E_y, E_z)$ and $\mathbf{H} = (H_x, H_y, H_z)$ designate, respectively, the electric and the magnetic wave-field, and Z_0 is the impedance of free space, $Z_0 = (\mu_0/\epsilon_0)^{1/2}$. In equation 1, $\tilde{T}$ is a 4×4 matrix that depends on the constitutive relation of the medium and on the direction of the incident wave. *Scarabucci* [1969] gives the elements of $\tilde{T}$ explicitly as functions of the parameters of a general ionosphere composed of a mixture of positive and negative ions embedded in a magnetic field. The elements of $\tilde{T}$ are functions of z because the medium parameters are supposed to vary along only the z axis.

Given the direction of the incident wave and the composition of the medium, the refractive index of the incident wave can be calculated and all the elements of $\tilde{T}$ can be determined for solving the characteristic equation

$$\det(\tilde{T} - q\tilde{I}) = 0 \tag{3}$$

where $\tilde{I}$ is a 4×4 unit matrix. Equation 3 gives four eigenvalues q_a, q_b, q_c, and q_d for $z < z_0$; similarly, it gives q_a', q_b', q_c', and q_d' for $z \geq z_1$. From the four eigenvalues q_a' to q_d' we select two that correspond to upgoing waves. Suppose these two upgoing eigenvalues q_a' and q_b' have been selected and that we obtain from them the two related eigenvectors $\mathbf{e}_{a'}$ and $\mathbf{e}_{b'}$ [see *Scarabucci*, 1969, append. B]. We begin with one eigenvector $\mathbf{e}_{a'}$, and at some point $z_i \geq z_1$ equation 1 is integrated backward by the use of a numerical integration procedure. For any point

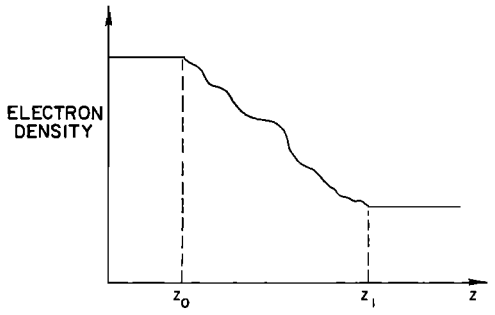

Fig. 2. Example of variable planar stratification when the variable parameter is the electron density. It is assumed that the medium is homogeneous for $z > z_1$ and for $z < z_0$.

at $z \leq z_0$ (homogeneous medium) the total field will be, in general, the composition of four waves (two incident and two reflected). For $z \leq z_0$ a spatial Fourier analysis is performed by which we obtain all the fields of the four possible waves (two incident, two reflected) that gave rise to $\mathbf{e}_{a'}$.

The above Fourier analysis with the wave fields and with the related derivatives that came out from the integration procedure is lengthy and is omitted here. Details of the process can be found in *Scarabucci and Smith* [1970].

An equal integration process is repeated for the other purely upgoing eigenvector $\mathbf{e}_{b'}$. Therefore we have now two independent solutions that can be combined to satisfy a new boundary condition, namely that the incident wave is a characteristic wave type a (i.e., $q_i = q_a$). All the wave fields are then obtained by the proper combination of the two solutions.

The above general full-wave integration process will be used for the simple geometry assumed in this paper.

5. STUDY OF MAGNETOSPHERIC FIELD ORIENTED IRREGULARITIES

Magnetospheric model. Consider the coordinate axes and the geometry of Figure 1. The assumption of a planarly stratified field-oriented electron-density irregularity is introduced by setting $DIP = 0$. Next, suppose that the azimuthal angle χ is equal to 180°; this condition characterizes propagation along the magnetic meridian with the y projection of $\mathbf{k}$ being opposite to $\mathbf{B}_0$.

The electron density profile along z will be assumed to be

$$N(z) = N_0 \qquad z \leq 0$$
$$N(z) = N_0 + \Delta N\left[\exp\left(-\frac{1}{2}\cdot\frac{z^2}{\sigma^2}\right) - 1\right] \qquad z > 0 \tag{4}$$

where N_0 is the electron density for $z \leq 0$, ΔN is the total change in N for $z \to \infty$, and the 'variance' σ measures the distance in which $N(z)$ changes by what is arbitrarily considered a 'considerable amount.' This expression for $N(z)$ is appropriate for the following mathematical treatment because by varying ΔN and σ we can approximately simulate a wide range of electron density irregularities. For example, $\sigma = 0$ corresponds to the problem of incidence on a sharp boundary discontinuity. On the other hand, the amount of excitation of the reflected and transmitted waves will depend on how σ compares with some suitable wavelengths. One example of an electron density profile is shown in Figure 3.

Simplification of the equations. For $DIP = 0$, $\chi = 180°$, and if we consider only the effect of electrons, the elements [e.g., *Scarabucci*, 1969] of the matrix $\tilde{T}$ reduce to:

$$\begin{aligned}
T_{11} &= T_{12} = T_{13} = 0 \\
T_{14} &= 1 \\
T_{21} &= jn_i SXY/\alpha \\
T_{22} &= 0 \\
T_{23} &= 1 - n_i^2 S^2(1 - Y^2)/\alpha \\
T_{24} &= 0 \\
T_{31} &= T_{33} = T_{34} = 0 \\
T_{32} &= 1 - X \\
T_{41} &= 1 - n_i^2 S^2 - X(1 - X)/\alpha \\
T_{42} &= T_{44} = 0 \\
T_{43} &= -T_{21}
\end{aligned} \tag{5}$$

where $\alpha = 1 - X - Y^2$.

Under the above conditions the Booker quartic reduces to a biquadratic equation

$$q^2 = A^2 - \left\{X\Big/\left[1 - \frac{A^2Y^2}{2(1-X)} \pm \left(\frac{A^4Y^4}{4(1-X)^2} + \frac{n_i^2S^2Y^2}{(1-X)}\right)^{1/2}\right]\right\} \tag{6}$$

where

$$A^2 = 1 - n_i^2 S^2 \tag{7}$$
$$S = \sin I \tag{8}$$
$$X = f_N^2/f^2 \tag{9}$$
$$Y = f_H/f \tag{10}$$

and n_i is the refractive index of the incident wave for $z \leq 0$. The quantities f_N and f_H represent the plasma frequency and the gyrofrequency, respectively:

$$f_N^2 \cong 8.061 \times 10^7 N \qquad (\text{Hz, cm}^{-3}) \tag{11}$$
$$f_H \cong 27.99 B_0 \qquad (\text{Hz, } \gamma) \tag{12}$$

and B_0 is given in gammas, $1\gamma = 10^{-9}$ weber /m^2.

Given the angle of incidence I and the parameters f_N and f_H for $z < 0$ the refractive index of the incident wave is determined and equation 6 gives the four values of q that correspond to four characteristic waves with the same variation along y, $\exp(-jkn_iSy)$. Two of the four values of q belong to upgoing waves: q_a corresponds to the incident wave and q_b corresponds to a second possible upgoing wave. The other two (q_c and q_d) correspond to reflected downcoming waves. Therefore, by solving the biquadratic equation (6) the spatial variation of all reflected and incident waves can be determined. Later we impose the condition that only one incident wave is present.

Similarly, for $z \gg \sigma$ the electron density will be

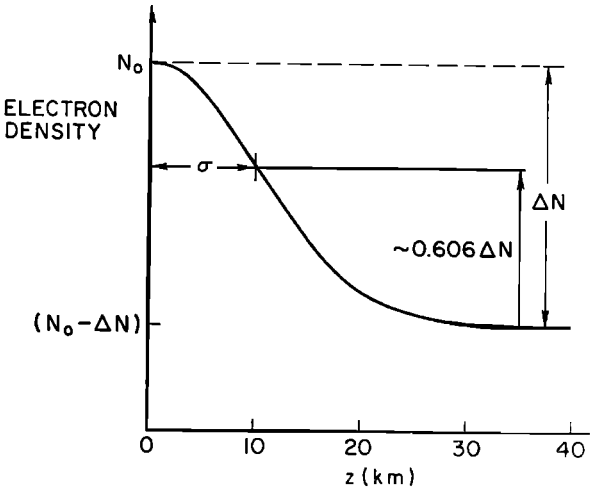

Fig. 3. The electron density profile. It is assumed that

$$N = N_0 + \Delta N\left[\exp\left(-\frac{1}{2}\cdot\frac{z^2}{\sigma^2}\right) - 1\right]$$

which corresponds to one half of a bell-shaped irregularity. σ is a measure of the distance in which the variation ΔN takes place; for $z = \sigma$ the electron density is approximately $(N_0 - 0.4\ \Delta N)$.

$N(z) \cong N_0 - \Delta N$ and (6) again will furnish four values of q. Here the boundary problem requires that the energy come from below and two eigenvalues (q_a' and q_b') must be selected that correspond to waves whose Poynting vector is directed upward. With the above upgoing eigenvalues and the use of the results of *Scarabucci and Smith* [1970], the following starting eigenvectors are deduced for $z \gg \sigma$:

$$\mathbf{e}_{a',b'} = \begin{bmatrix} E_x \\ -E_y \\ Z_0 H_x \\ Z_0 H_y \end{bmatrix} \quad \text{at} \quad z \gg \sigma \tag{13}$$

such that

$$E_y = \frac{jn_i S X Y q}{(1 - X - Y^2)(1 - X - q^2) - n_i^2 S^2 (1 - Y^2)(1 - X)} \cdot E_x \tag{14}$$

$$Z_0 H_x = \frac{-jn_i S X Y (1 - X)}{(1 - X - Y^2)(1 - X - q^2) - n_i^2 S^2 (1 - Y^2)(1 - X)} \cdot E_x \tag{15}$$

$$Z_0 H_y = q E_x \tag{16}$$

for $q = q_a'$ and $q = q_b'$.

Given a starting eigenvector at $z_i \gg \sigma$ the set of linear differential equations (1) can be numerically integrated from z_i to $z_k < 0$. With the two starting eigenvectors two independent solutions are constructed. For each solution the value of $\mathbf{e}$ at each point represents the sum of four waves, two upgoing and two downcoming waves. A spatial Fourier analysis is then made for $z < 0$ where the medium is homogeneous (as explained in section 4). When the propagation is along the magnetic meridian the values of q that correspond to downcoming waves have the same amplitudes but opposite signs of the q's that correspond to upgoing waves; this pattern is a result of (3). Then the spatial Fourier analysis is simplified as explained below.

The total field E_x is a sum of four x-fields:

$$\begin{aligned} E_x(z) &= U_{xa}(z) + U_{xb}(z) + D_{xa}(z) + D_{xb}(z) \\ &= U_{xa} e^{-jkq_a z} + U_{xb} e^{-jkq_b z} + D_{xa} e^{jkq_a z} \\ &\quad + D_{xb} e^{jkq_b z} \end{aligned} \tag{17}$$

where $U_{xa}(z)$ and $U_{xb}(z)$ denote upgoing and $D_{xa}(z)$, $D_{xb}(z)$ denote downcoming x-electric fields, respectively.

For the derivative d/dz we have

$$\frac{E_x'(z)}{-jk} = q_a U_{xa} e^{-jkq_a z} + q_b U_{xb} e^{-jkq_b z} - q_a D_{xa} e^{jkq_a z} - q_b D_{xb} e^{jkq_b z} \tag{18}$$

Let us then take two points z_1 and z_{01} such that

$$kq_a(z_1 - z_{01}) = 2\pi \tag{19}$$

Define

$$\beta = kq_b(z_1 - z_{01}) = 2\pi \cdot q_b/q_a \tag{20}$$

$$\Delta E_x = E_x(z_1) - E_x(z_{01}) \tag{21}$$

$$\Delta E_x' = E_x'(z_1) - E_x'(z_{01}) \tag{22}$$

With the above definitions it can be deduced that the x-electric fields are given by

$$U_{xb}(z_1) = \frac{1}{2(1 - e^{i\beta})} \cdot \left(\Delta E_x - \frac{\Delta E_x'}{jkq_b} \right) \tag{23}$$

$$D_{xb}(z_1) = \frac{1}{2(1 - e^{-i\beta})} \cdot \left(\Delta E_x + \frac{\Delta E_x'}{jkq_b} \right) \tag{24}$$

$$U_{xa}(z_1) = (1/2)(P_1 + P_2) \tag{25}$$

$$D_{xa}(z_1) = (1/2)(P_1 - P_2) \tag{26}$$

where

$$P_1 = E_x(z_1) - D_{xb}(z_1) - U_{xb}(z_1) \tag{27}$$

$$P_2 = -\frac{E_x'(z_1)}{jkq_a} - \frac{q_b}{q_a} [U_{xb}(z_1) - D_{xb}(z_1)] \tag{28}$$

Similar equations are found for the y fields. Hence, upgoing and downcoming waves are determined for each independent solution. Now if we use the fact that the incident wave is a pure characteristic wave type a (say) it is possible to find all the fields, as shown in *Scarabucci and Smith* [1970].

Numerical analysis. The full-wave technique has been applied for analyzing some cases that are representative of magnetospheric irregularities. As an example we chose the parameters

$$f_{N0} = 100\ \text{kHz}$$
$$f_H = 20\ \text{kHz} \qquad (29)$$
$$f = 5\ \text{kHz}$$
$$\Delta N = \Delta X = 10\%$$

This example represents some region in the magnetosphere where a relatively small variation (10%) of ionization is found. The refractive index surfaces for the two media are shown in Figure 4. Medium 1 corresponds to the region $z < 0$, where the electron density is N_0; medium 2 corresponds to $z \gg \sigma$, where the density is $(N_0 - \Delta N)$. Suppose the incident waves makes an angle I with the vertical. The refractive index for this wave is represented by the vector that forms an angle I with the vertical and that touches the corresponding refractive index surface (see Figure 4) as indicated. The vertical projection of this vector is the root of the Booker quartic that corresponds to the incident wave. Set $q = q_a$

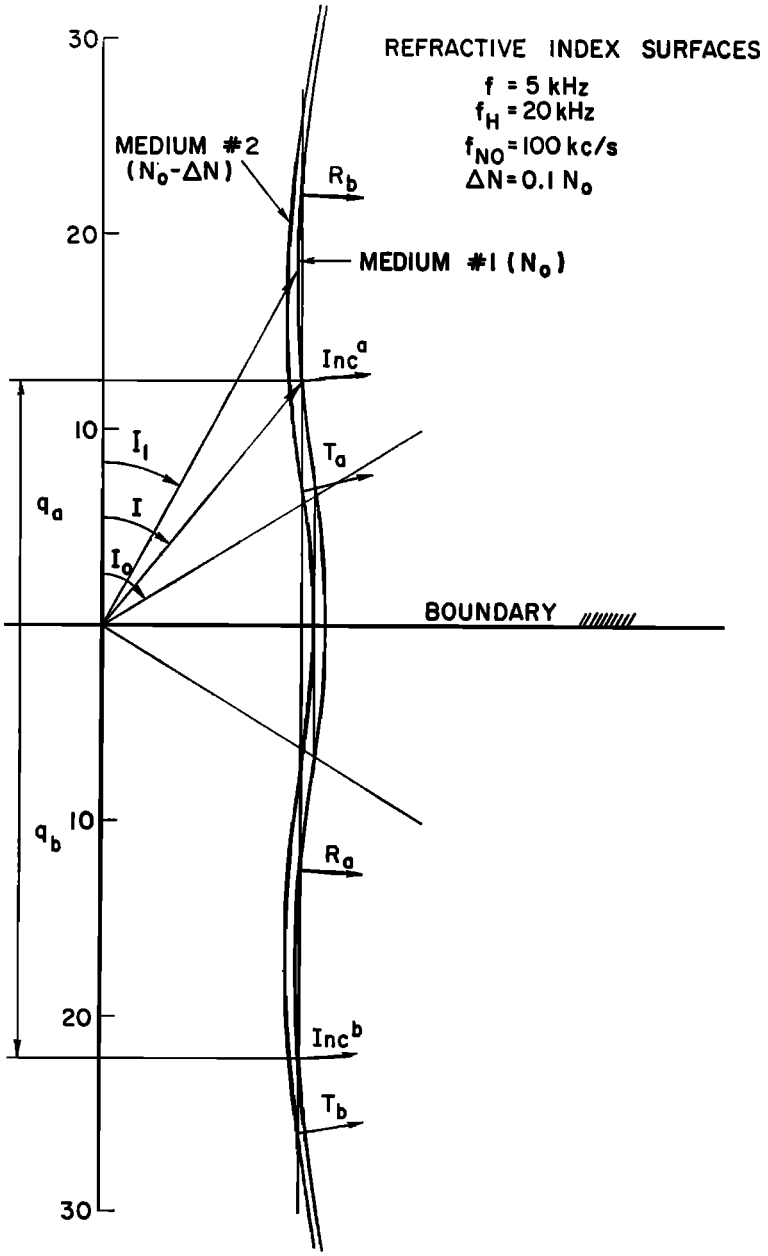

Fig. 4. Refractive index surfaces for the two media. (see text).

and arbitrarily define the incident wave as being a type a wave. The energy flow direction is perpendicular to the refractive index surface. Hence, the group velocity of the incident wave is along Inc^a. More precisely, waves with the refractive index vector and the group velocity directed toward the same region are defined as type a waves. Inversely, if the phase velocity and the group velocity are directed toward different regions the wave is defined as a backward b wave. For example, there are type a waves for $I \geq I_1$ and type b waves for $I < I_1$ (I_1 is the angle for which $\partial(n_\phi S)/\partial I = 0$ in the refractive index curve of Figure 4). Observe that the backward b waves correspond to the higher values of $|q|$.

To satisfy Snell's law the incident wave will give rise to transmitted waves in medium 2 that have group velocities along T_a and T_b and that have reflected waves in medium 1 whose group velocities will be along R_a and R_b. Line Inc^b corresponds to the other possible incident wave with the same $n_\phi S$ projection on the boundary. Notice that q_b is negative.

If now the angle of incidence is allowed to increase we observe that the root of the Booker quartic corresponding to T_a decreases and finally passes through zero at $I = I_0$ ($I_0 \cong 57°$ in our example). If $I > I_0$ the corresponding q becomes imaginary and the wave will be evanescent. Hence, for $I > I_0$ only a backward b wave can be found at $z \gg \sigma$ because the other possible transmitted wave is evanescent.

The use of refractive index surfaces gives the possible reflected and transmitted wave and ray directions but does not give the actual amplitudes of the fields. For this we need a full-wave solution. The result provided by the full-wave computer program

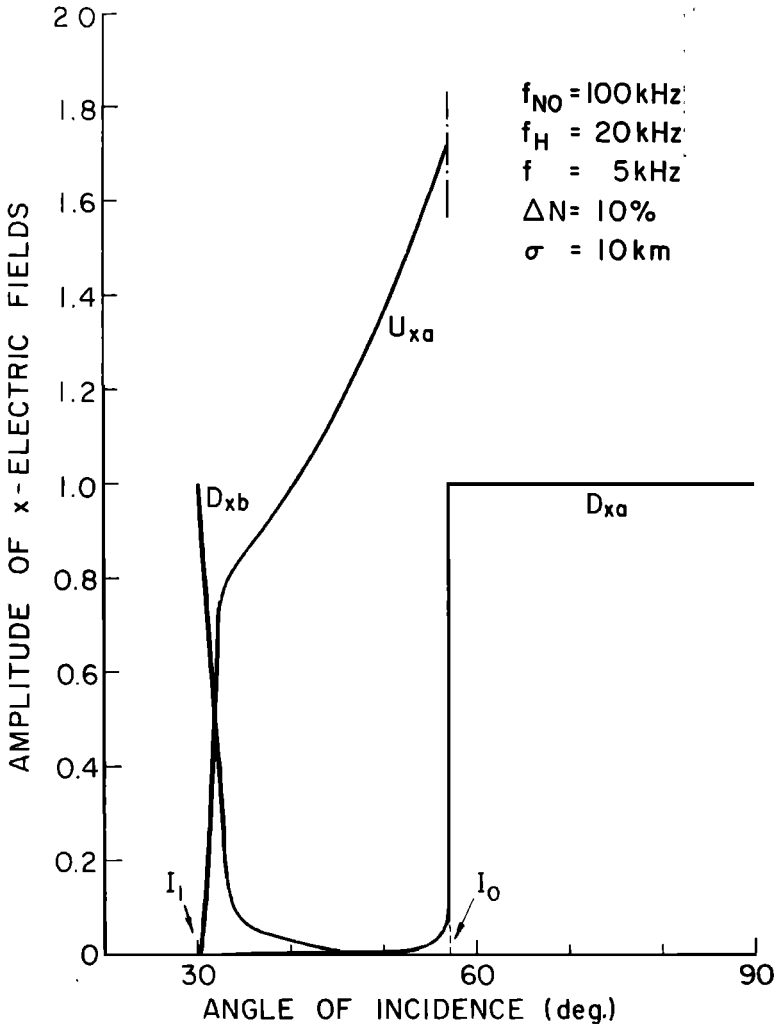

Fig. 5. Amplitude of the x electric fields coming out of the boundary region as a function of the angle of incidence. The incident x electric field has unit amplitude.

is shown in Figure 5, where the x-electric wave-field amplitude is plotted as a function of I for the parameters given in (29) and for $\sigma = 10$ km. The incident wave is a type a wave with x electric field of unit amplitude. D_{xa} and D_{xb} are the x-electric field amplitudes of the reflected type a and type b waves, respectively. Similarly, U_{xa} and U_{xb} are the corresponding amplitudes for the upgoing T_a and T_b waves.

Figure 5 shows that D_{xa} exhibits a jump at $I = I_0 \cong 57°$. If $I > I_0$, the incident wave will excite almost only a reflected wave whose characteristics are the same as those of the incident wave. For $I < I_0$, D_{xa} decreases very steeply, as shown in Figure 5. The transmitted wave-field U_{xa} decreases when I decreases; it goes to zero at I_1 because there is no incidence of energy on the boundary when the incident k vector makes an angle I_1 with the vertical. The downcoming wave that will be excited for decreasing values of I is the backward b wave D_{xb}. At $I = I_1$ the 'incident' wave type a in fact corresponds to the 'reflected' wave type b; therefore, $D_{xb} = 1$. The backward upgoing wave U_{xb} is negligible compared with the others and is not noticeable in Figure 5.

Angles of incidence smaller than I_1 have not been considered because they represent backward waves whose energy never hits the boundary at $z = 0$. For angles of incidence equal to $(180° - I)$, $I < I_1$, there are backward b waves like the one represented by Inc^b in Figure 4, which can be considered an incident wave. These waves are not treated here, but the full-wave result is: excitation with a backward wave gives rise to almost only transmitted waves of the same type (i.e., $Inc^b \rightarrow T_b$).

Figure 6 shows the power flux coefficients for the

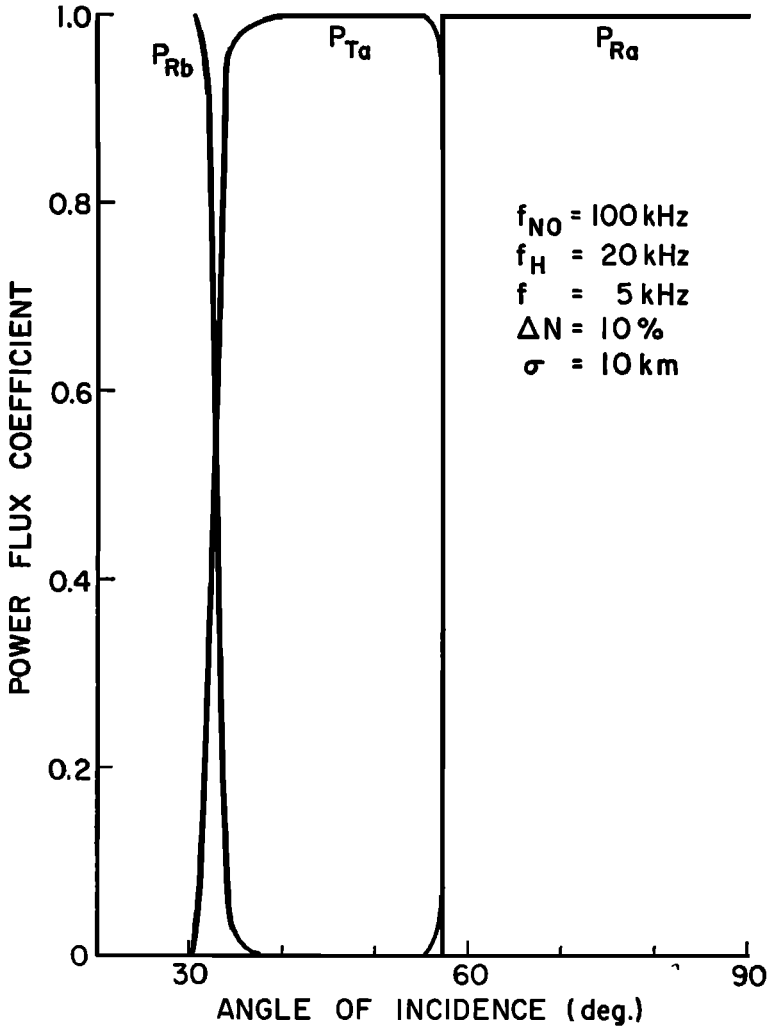

Fig. 6. Power flux coefficients for the wave fields shown in Figure 5.

waves whose electric fields are shown in Figure 5. The power flux coefficient of one wave is defined as the ratio between the power flux in this wave and the sum of all power fluxes coming out of the boundary region. Figure 6 is self-explanatory.

Instances in which the transmitted type a wave is evanescent in the second medium are of special interest because they represent the natural possibility of ducting in the magnetosphere. Figure 7 shows the total instantaneous x-electric field as a function of height z, for $I = 60°$. The parameters are the same as for Figure 5. Figure 7 shows an almost perfect reflection with the electric field behaving as in the situation when there is a linear gradient of electron density and the medium is isotropic. The form of the field with z resembles very much an Airy integral function and is closely related to the Stokes phenomenon [see *Budden,* 1961, chap. 15, 16]. For the medium parameters shown in Figure 7 the excitation of the high-q backward waves is negligible compared with the amplitude of the reflected wave type a. Therefore, the incident wave type a (for which $q = +q_a$) gives rise to almost only the reflected wave type a (for which $q = -q_a$).

The amplitude of the x electric fields of the high-q backward waves is of the order of 1/1000 in the

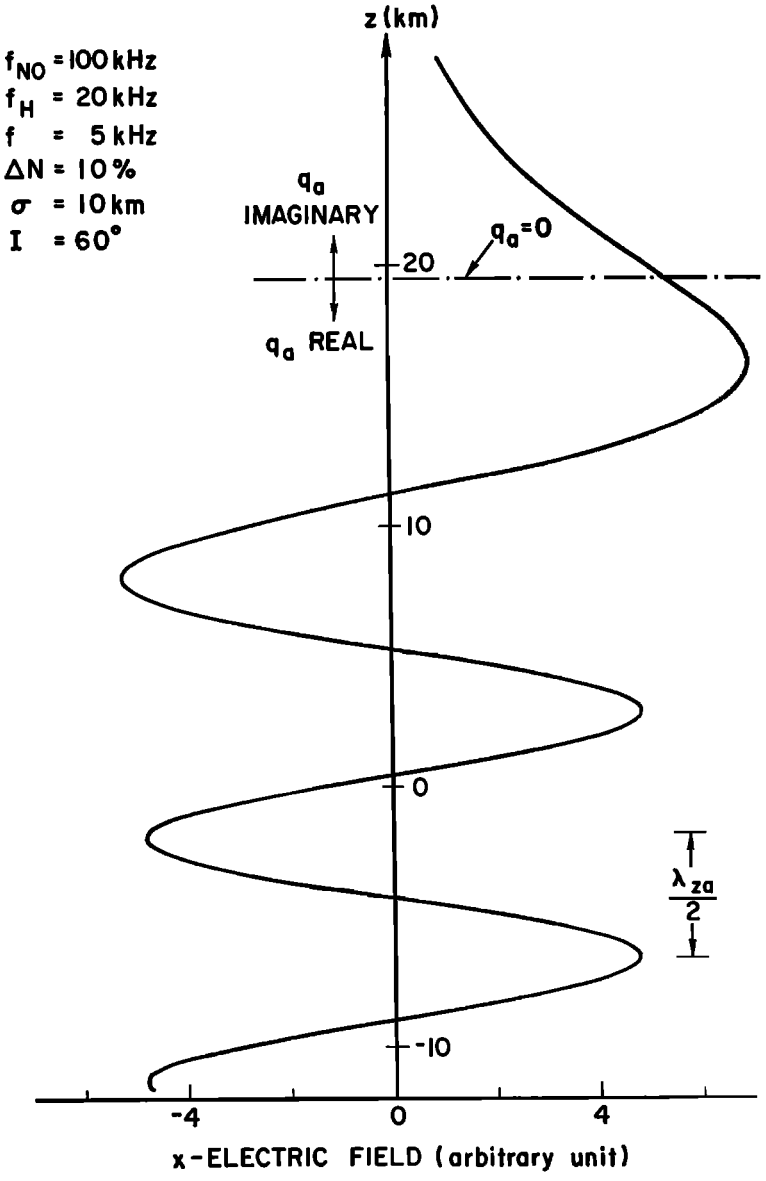

Fig. 7. Instantaneous x electric field as a function of the height z. Medium parameters are shown in the figure and $I = 60°$. One quarter of a period later the field is zero everywhere and one half a period later the field will be the negative of the field shown in the figure. It is a standing wave.

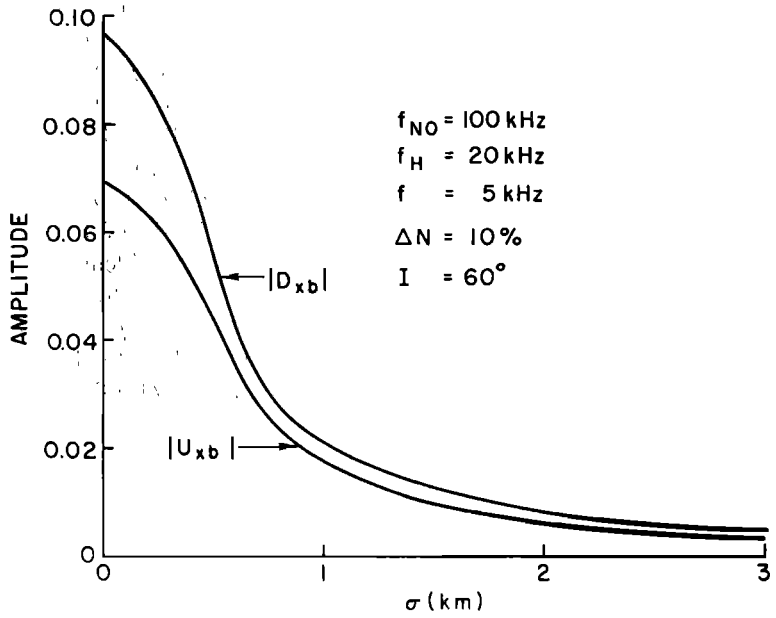

Fig. 8. Amplitude of the x electric fields for the high-q backward waves as a function of the thickness parameter σ. Other parameters were kept constant as in Figure 7.

example of Figure 8; therefore, they are not noticeable in that figure. One-quarter of a period later the instantaneous x electric field would be approximately zero everywhere, and one-half a period later it would be the negative of the field shown in Figure 7. The distance between two consecutive maximums for $z < 0$ is equal to $\lambda_{za}/2$, where λ_{za} is the wavelength in the z direction for the wave type a; i.e.,

$$\lambda_{za} = 2\pi/kq_a = \lambda_0/q_a \tag{30}$$

and λ_0 is the free space wavelength.

Hence, Figure 7 shows that a small variation in ionization can effectively work as a perfect reflector, depending on the frequency and the angle of incidence of the wave.

If the thickness parameter σ is equal to 10 km, then only one type a wave is reflected under the conditions shown in Figure 7. For smaller values of σ it would be important to know the amplitudes of the backward transmitted and reflected b waves generated at the discontinuity. This result is shown in Figure 8, where the amplitudes of the upgoing transmitted U_{xb} and downcoming reflected D_{xb} x-electric fields are taken as a function of σ. The other parameters were kept constant, as in Figure 7. The maximum power excitation for the b waves (transmitted and reflected) occurs for $\sigma = 0$, i.e., for sharp boundary. If we set a value of 100 for the z component of the power flow carried by the reflected type a waves, the values of $|D_{xb}|$ and $|U_{xb}|$ displayed in Figure 8 for $\sigma = 0$ correspond, respectively, to power flow values of 14.3 and 10.8. Compare now the result of Figure 8 with the values of the wavelengths along z.

Incident and reflected wave type a:

$$\lambda_{za} = \frac{\lambda_0}{q_a} = \frac{60}{6.3965} \cong 9.4 \text{ km}$$

Reflected wave type b:

$$\lambda_{zb} = \frac{\lambda_0}{|q_b|} = \frac{60}{28.7048} \cong 2.09 \text{ km}$$

Transmitted wave type b:

$$\lambda_{zb'} = \frac{\lambda_0}{|q_{b'}|} = \frac{60}{30.6986} \cong 1.95 \text{ km}$$

We conclude that the amount of high-q backward waves excited at the discontinuity depends on how σ compares with the smallest z-wavelengths of these modes. Fortunately, the desired mode has the longer z-wavelength. The amount of excitation is negligible for $\lambda_{zb}, \lambda_{zb'} \ll \sigma$ and becomes appreciable (but still small in the example of Figure 8) for small values of σ, i.e., for steeper variation of ionization. This result is in fact predicted when a detailed study is made of the related coupled wave equations.

Coupled wave equations. *Budden and Clemmow* [1957] showed that the set of equations (1) can be transformed into a new set of first-order coupled equations expressed in terms of the ionospheric pa-

rameters. Here the notation of Budden and Clemmow will be used; however, the fact that our coordinate axes are different from the ones used by them will be taken into account.

To transform equations 1 into a set of first-order coupled equations, we allow the roots of the Booker quartic equation to be functions of z. After a lengthy matrical manipulation in linear space the set (1) is transformed into the following set of first-order coupled equations (a prime denotes d/dz):

$$\mathbf{g}' + jk\tilde{\Delta}\cdot\mathbf{g} = \tilde{\Gamma}_1\cdot\mathbf{g} \tag{31}$$

where

$$\mathbf{g} = \begin{bmatrix} g_1 \\ g_2 \\ g_3 \\ g_4 \end{bmatrix} \tag{32}$$

$$\tilde{\Delta} = \begin{bmatrix} q_a & 0 & 0 & 0 \\ 0 & -q_a & 0 & 0 \\ 0 & 0 & q_b & 0 \\ 0 & 0 & 0 & -q_b \end{bmatrix} \tag{33}$$

$$\tilde{\Gamma}_1 = \begin{bmatrix} -\frac{q_a'}{2q_a} & \frac{\chi}{\rho_0} + \frac{q_a'}{2q_a} & -\frac{\chi}{2}\left(1-\frac{q_b}{q_a}\right)-\frac{\psi}{2}\left(1+\frac{q_b}{q_a}\right) & -\frac{\chi}{2}\left(1+\frac{q_b}{q_a}\right)-\frac{\psi}{2}\left(1-\frac{q_b}{q_a}\right) \\ \frac{\chi}{\rho_0} + \frac{q_a'}{2q_a} & -\frac{q_a'}{2q_a} & -\frac{\chi}{2}\left(1+\frac{q_b}{q_a}\right)-\frac{\psi}{2}\left(1+\frac{q_b}{q_a}\right) & -\frac{\chi}{2}\left(1-\frac{q_b}{q_a}\right)-\frac{\psi}{2}\left(1+\frac{q_b}{q_a}\right) \\ \frac{\chi}{2}\left(1-\frac{q_a}{q_b}\right)-\frac{\psi}{2}\left(1+\frac{q_a}{q_b}\right) & \frac{\chi}{2}\left(1+\frac{q_a}{q_b}\right)+\frac{\psi}{2}\left(\frac{q_a}{q_b}-1\right) & -\frac{q_b'}{2q_b} & \frac{\chi}{\rho_z} + \frac{q_b'}{2q_b} \\ \frac{\chi}{2}\left(1+\frac{q_a}{q_b}\right)+\frac{\psi}{2}\left(\frac{q_a}{q_b}-1\right) & \frac{\chi}{2}\left(1-\frac{q_a}{q_b}\right)-\frac{\psi}{2}\left(1+\frac{q_a}{q_b}\right) & -\frac{\chi}{\rho_z} + \frac{q_b'}{2q_b} & -\frac{q_b'}{2q_b} \end{bmatrix} \tag{34}$$

The g's are linear combinations of E_x, E_y, H_x, and H_y (see (39) to (42)). Each g represents one distinct wave. For a homogeneous medium the vector $\mathbf{g}$ corresponds to four independent progressive plane waves, the characteristic waves. This occurs because all the elements of $\tilde{\Gamma}_1$ depend on spatial derivatives of the medium parameters which vanish in a homogeneous medium. In an inhomogeneous medium the equations lose their mutual independence and the additional terms are related to coupling between them. For example, reflection is a special case of coupling. In the above equations, q_a and q_b are solutions of the Booker quartic (3) and are functions of z. The elements Γ_{ij} are related to ionospheric parameters; therefore, they also are z dependent functions. For propagation in the magnetic meridian the terms χ, ρ_0, ρ_z, and ψ are related to the ionospheric parameters by the following expressions:

$$2\chi = X' \Big/ \left\{(X-1)\cdot\left[\frac{Y^2A^4}{(X-1)n_i^2S^2} - 4\right]^{1/2}\right\} \tag{35}$$

$$2\rho_0 = \frac{YA^2}{n_iS(X-1)^{1/2}} + \left[\frac{Y^2A^4}{n_i^2S^2(X-1)} - 4\right]^{1/2} \tag{36}$$

$$\psi = \frac{\rho_0'}{2(\rho_0 - \rho_z)}\left\{\frac{YA^2}{n_iS(X-1)^{1/2}} - \left[\frac{Y^2A^4}{n_iS(X-1)} - 4\right]^{1/2}\right\} \tag{37}$$

$$\rho_z = 1/\rho_0 \tag{38}$$

The new variables g_i are linear combinations of the variables E_x, E_y, Z_0H_x, and Z_0H_y:

$$g_1 = \frac{1}{[2(\rho_0^2 - 1)]^{1/2}}\left[\rho_0E_x + \frac{j(X-1)^{1/2}}{q_a}E_y + \frac{jZ_0H_x}{(X-1)^{1/2}} + \frac{\rho_0}{q_a}Z_0H_y\right] \tag{39}$$

$$g_2 = \frac{1}{[2(\rho_0^2 - 1)]^{1/2}}\left[\rho_0E_x - \frac{j(X-1)^{1/2}}{q_a}E_y + \frac{jZ_0H_x}{(X-1)^{1/2}} - \frac{\rho_0}{q_a}Z_0H_y\right] \tag{40}$$

$$g_3 = \frac{1}{[2(1 - \rho_z^2)]^{1/2}}\left[\rho_zE_x + \frac{j(X-1)^{1/2}}{q_b}E_y + \frac{jZ_0H_x}{(X-1)^{1/2}} + \frac{\rho_z}{q_b}Z_0H_y\right] \tag{41}$$

$$g_4 = \frac{1}{[2(1 - \rho_x^2)]^{1/2}} \left[\rho_x E_x - \frac{j(X-1)^{1/2}}{q_b} E_y + \frac{jZ_0 H_x}{(X-1)^{1/2}} - \frac{\rho_x}{q_b} Z_0 H_y \right] \quad (42)$$

In (31) the terms Γ_{ij}, $i \neq j$ represent coupling between the several waves. Figures 9, 10, and 11 show some coupling coefficients when the thickness parameter σ is allowed to vary. The medium parameters and the angle of incidence are the same as in Figure 8. Figure 9 shows that the coupling coefficient ψ is in general very small for values of σ greater than four, with a behavior pattern strongly influenced by dN/dz. A similar curve is shown in Figure 10, in which χ/ρ_0 is plotted as a function of z/σ. For the conditions of Figure 8, ρ_0 is a very slowly varying function with values of approximately 0.6.

Figure 11 shows the 'self coupling' coefficient $q'_a/2q_a$. It also gives roughly the coupling between the incident wave type a and the reflected wave of the same type. Figure 11 shows that this coupling is infinite at $q_a = 0$ and, furthermore, that the WKB method can be used up to a value of z near where $q_a = 0$ if σ is much greater than four.

The second-order coupled equations are deduced from (31) by introducing new variables

$$h_1 = \frac{1}{\sqrt{2}}(g_1 + g_2) = \frac{1}{(\rho_0^2 - 1)^{1/2}} \cdot \left[\rho_0 E_x + \frac{jZ_0 H_x}{(X-1)^{1/2}} \right] \quad (43)$$

$$h_3 = \frac{1}{\sqrt{2}}(g_3 + g_4) = \frac{1}{(1 - \rho_x^2)^{1/2}} \cdot \left[\rho_x E_x + \frac{jZ_0 H_x}{(X-1)^{1/2}} \right] \quad (44)$$

as shown by *Budden and Clemmow* [1957]. They are

$$h_1'' + \left[k^2 q_a^2 + \psi^2 + \frac{\eta''}{\eta(\rho_0^2 - 1)} \right] h_1 = \left[-\psi' + \frac{\eta'' \rho_0}{\eta(\rho_0^2 - 1)} \right] h_3 - 2\psi h_3' \quad (45)$$

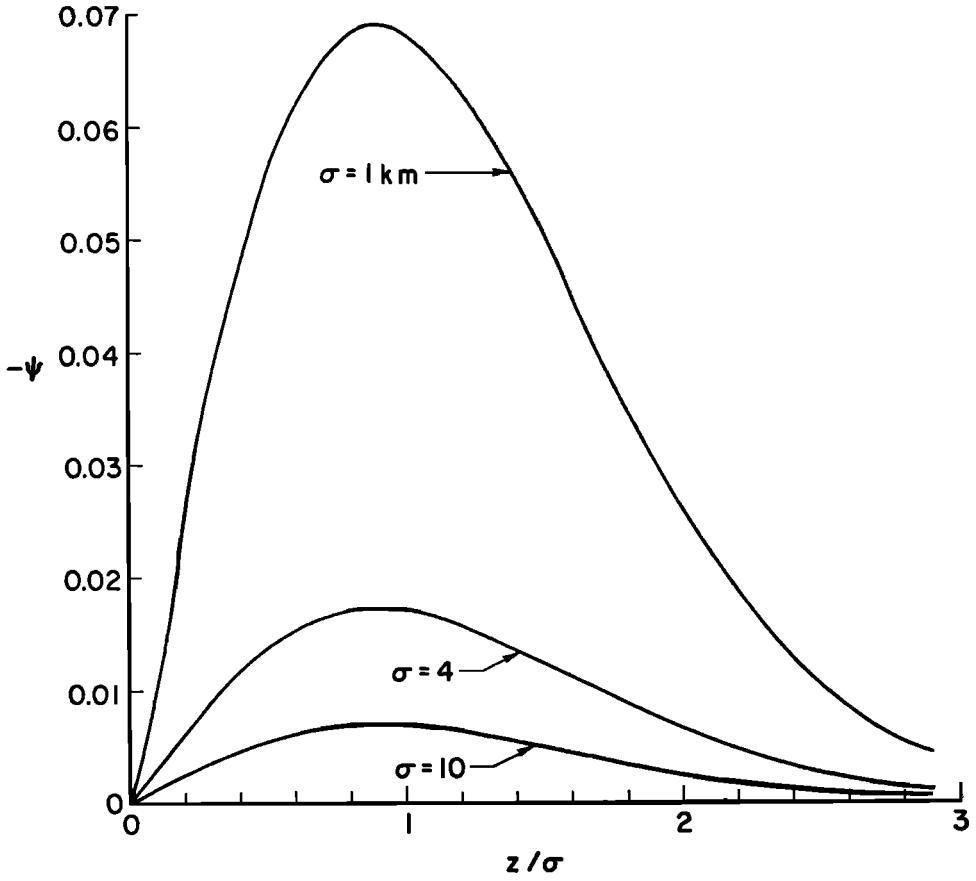

Fig. 9. The coupling coefficient ψ as a function of the height and parametric in σ.

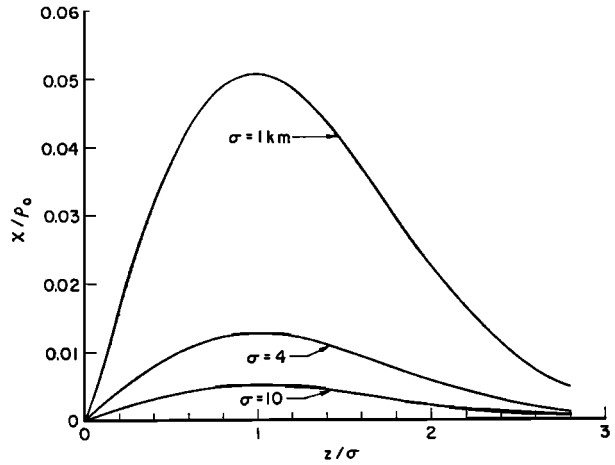

Fig. 10. The coupling coefficient χ/ρ_0 as a function of the height and parametric in σ.

$$h_3'' + \left[k^2 q_b^2 + \psi^2 + \frac{\eta''}{\eta(\rho_x^2 - 1)}\right] h_3 = \left[-\psi' + \frac{\eta'' \rho_x}{\eta(\rho_x^2 - 1)}\right] h_1 - 2\psi h_1' \qquad (46)$$

where

$$\frac{\eta''}{\eta} = -(\rho_0^2 - 1)\cdot\left(\frac{\chi}{\rho_0}\right)' + \chi^2 \frac{(\rho_0^2 - 1)^2}{\rho_0^2} - 2\chi\psi(\rho_0^2 - 1) \qquad (47)$$

After some mathematical manipulation and with the assumption that $X \gg 1$ it is possible to show that

$$\frac{\eta''}{\eta} = \frac{3}{4}\left(\frac{X'}{X}\right)^2 - \frac{1}{2}\left(\frac{X''}{X}\right) \qquad (48)$$

if the thickness parameter σ is greater than 4 km, and for the medium parameters shown in Figure 8 the term η''/η is much smaller than $k^2 q_a^2$ for any point z outside a very small interval containing the point where q_a passes through zero. Also, the coupling coefficient ψ is negligible as shown in Figure 9. Under this circumstance the terms multiplying h_3 and h_3' in (45) are very small in comparison with the terms that multiply h_1. Hence the coupling between h_1 and h_3 is negligible; it allows the approximation

$$h_1'' + k^2 q_a^2 h_1 \cong 0 \qquad q_a \neq 0 \qquad (49)$$

Observe that h_1 is a combination of the incident and reflected waves type a and that h_3 is a combination of upgoing and downcoming high-q backward waves.

Now, if σ is greater than ~4 km, Figure 11 shows that the WKB method can be used up to near the value of z that corresponds to

$$X = A^2(1 - Y) \qquad (50)$$

which is the point where q_a^2 passes through zero. Near this point q_a^2 can be linearized; hence the solution of (49) will be an Airy integral function [see Budden, 1961, sect. 16.8]. Hence the combination incident-reflected wave will be approximately given by an Airy integral function as shown in Figure 7. For small values of σ the total field departs considerably from the Airy integral function because the excitation of high-q backward waves becomes appreciable. This rules out the approximations that led to (49); therefore, incident and reflected a waves do not attain an Airy integral function behavior. One example is shown in Figure 12 for $\sigma = 1$ km. Figure 12 shows the instantaneous x-electric field as a function of z for the parameters displayed in the figure. The broken-line curve represents the total x electric field a quarter of a period later. A small-amplitude wave now penetrates the boundary region.

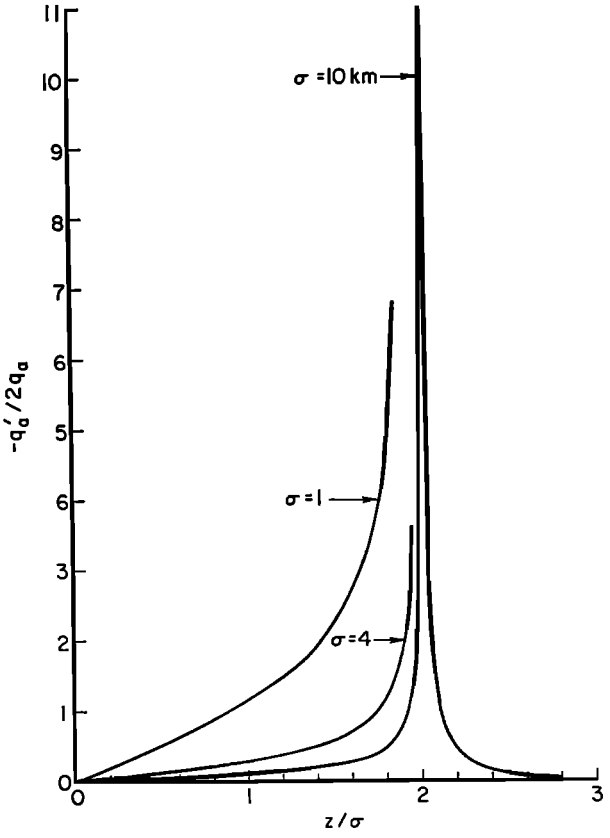

Fig. 11. The coupling coefficient $q_a'/2q_a$ as a function of the height and parametric in σ.

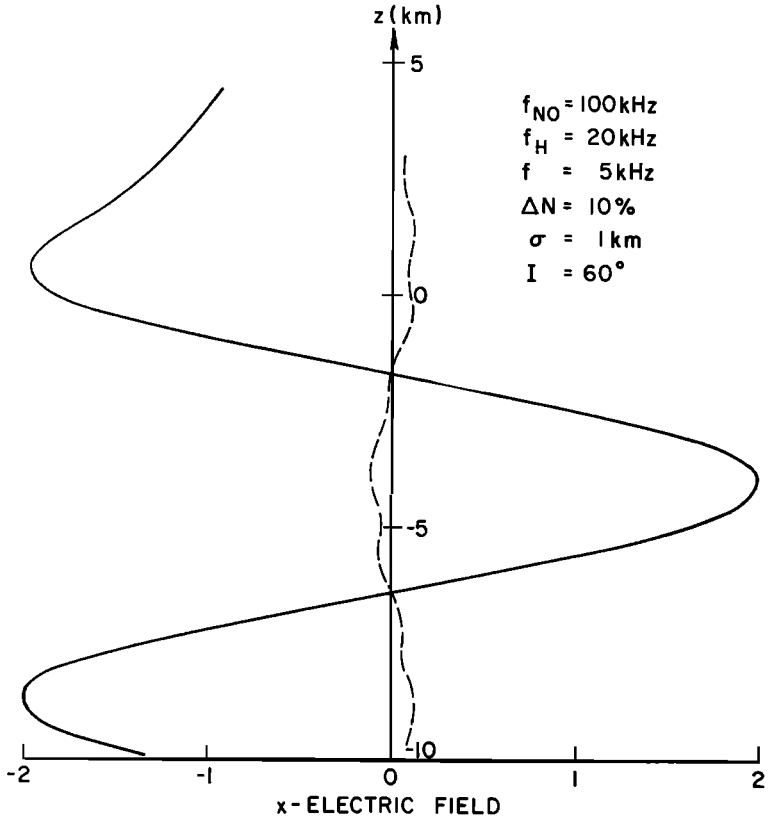

Fig. 12. Instantaneous x electric field as a function of the height z. Medium parameters are shown in the figure and $I = 60°$. The dashed curve represents the total x electric field one quarter of a period later. A small amplitude wave now penetrates the boundary region and then no standing wave is present.

6. MODE THEORY OF BELL SHAPED DUCTS

A natural result of the study developed in section 5 is a mode theory for propagation of plane waves inside bell shaped ducts. For deriving the mode theory it is necessary only to study the reflection coefficient for the type a wave at the point $z = 0$ (see Figure 3).

Determination of the modes. Suppose we start with a specific half part of a bell shaped irregularity as shown in Figure 3. Suppose that for certain values of frequency and angle of incidence the wave-field integration is followed by the spatial Fourier decomposition of the reflected waves at $z = 0$. Define now the reflection coefficient

$$R_a = \left.\frac{D_{xa}}{E_{x\,\mathrm{inc}}}\right|_{z=0} \tag{51}$$

The variable $E_{x\,\mathrm{inc}}$ is the x electric field of the incident wave type a. Therefore R_a gives the amplitude and the phase of the reflected wave type a that is generated by the upgoing incident wave of the same kind. Suppose that the existing homogeneous medium for $z < 0$ is replaced by the other symmetric part of the bell shaped profile, thereby developing a bell shaped duct. Then, the condition for having a mode inside this symmetric duct will be that

$$Ra \cdot Ra = |Ra|^2 \cdot e^{-2jn\pi} \tag{52}$$

that is

$$\angle Ra = -n\pi \tag{53}$$

where $n = 0, 1, 2, \cdots$.

Equation 52 states that the total change of phase in the z direction, as the waves move twice across the duct, must be an integral multiple of 2π for the mode to be self consistent. Hence, after finding the phase of the reflection coefficient Ra for several angles of incidence we can select the angles for which (53) is satisfied for $n = 0, 1, 2, \cdots$. These particular angles of incidence define the wave-guide modes inside the duct. Figure 13 is one example of the above procedure in which the wave-guide modes have been determined for a particular duct (see figure) and for $f = 5$ kHz. In this particular example we determined all the modes up to $n = 6$. Figures 14 and 15 show the E_x fields that result from the numerical full-wave solutions for $n = 0$ and $n = 4$.

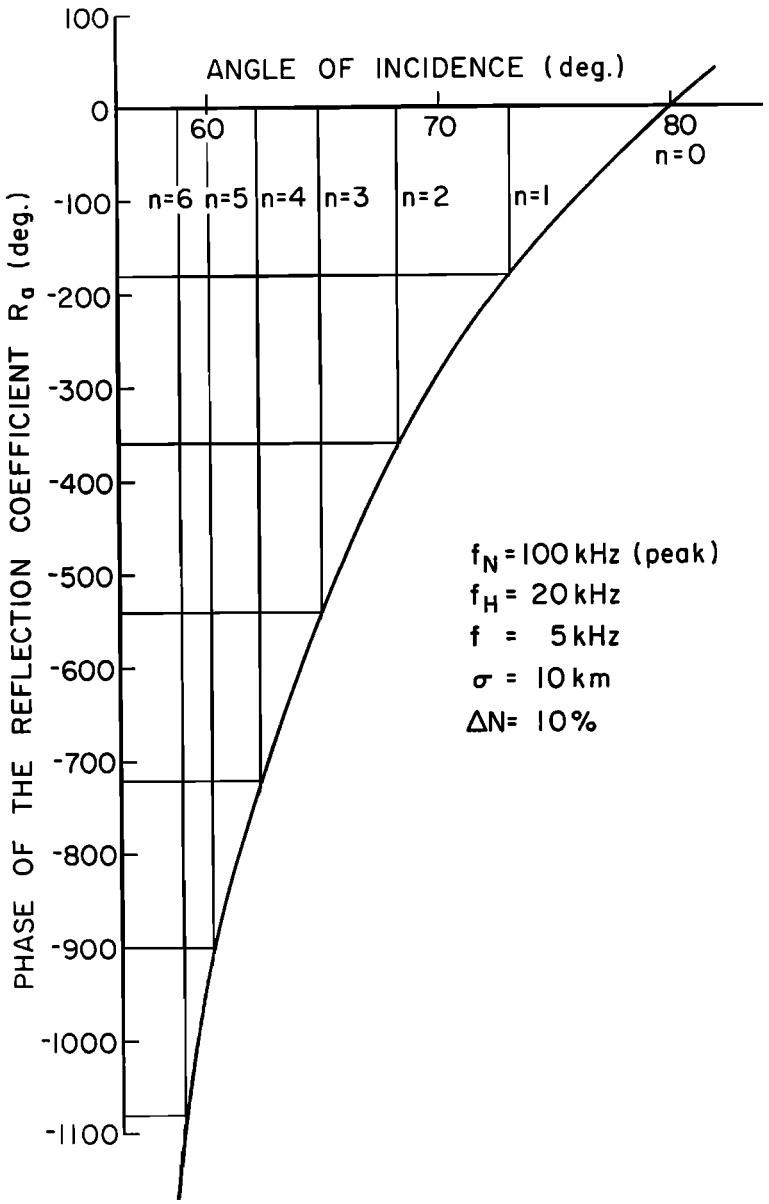

Fig. 13. Phase variation of the reflection coefficient *Ra* as a function of the angle of incidence. Lines $n = 1, 2$, et cetera, show how the modes are determined.

They correspond, respectively, to $I = 80°$ and $62°$ for the particular duct and frequency assumed. Observe the similarity of these fields to the probability density functions that result from the solution of the Schrodinger wave equation for the harmonic oscillator.

The higher modes correspond to steeper incidence; as a result, the width in which the mode is confined (measured by the points where q_a passes through zero) increases with n. This pattern is evident in Figures 14 and 15. As the angle of incidence decreases (steeper incidence) the point where q_a goes to zero occurs for higher values of z. Also there is an angle for which q_a no longer passes through zero. This is the point where D_{xa} jumps from ~ 1 to almost zero in Figure 5. For still lower angles of incidence the wave will no longer be trapped.

Now, we know from section 5 that the excitation of high-q backward waves is negligible for the medium parameters shown in Figure 13. Under this condition, a comparison between the full-wave method and the phase-integral method can be made. For the behavior of $q(X)$ presented here it can be shown [*Walker*, 1966*a*] that:

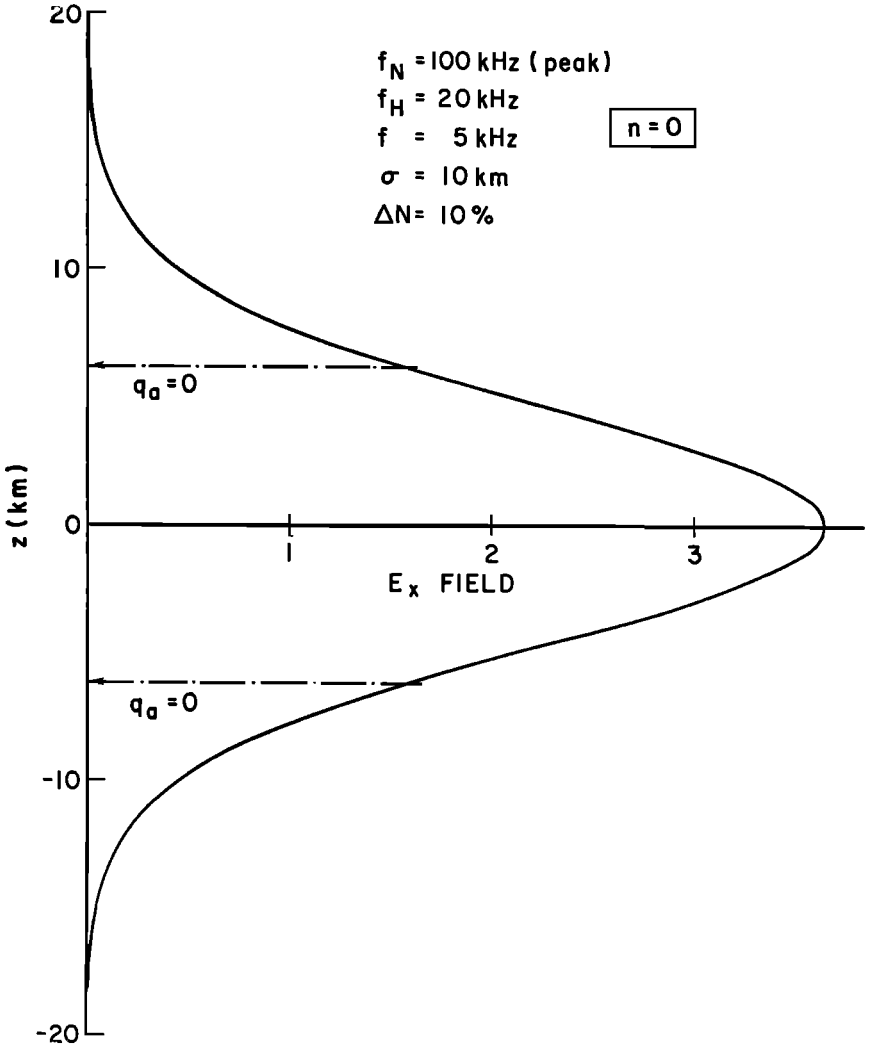

Fig. 14. Instantaneous x-electric field for the mode $n = 0$. One quarter of a period later the x field will be zero everywhere and one half a period later it will be the negative of the above field. Also shown are the points where $q_a = 0$. $I = 80°$ (from Figure 13).

$$Ra \cong j \exp\left(-2jk \int_0^{z_0} q\,dz\right) \tag{54}$$

and from (53) the condition for the mode to be self consistent is that

$$\frac{\pi}{2} - 2k \int_0^{z_0} q\,dz = -n\pi \tag{55}$$

or

$$Int = 2k \int_0^{z_0} q\,dz = (n + \tfrac{1}{2})\pi \tag{56}$$

In equations 54–56, z_0 is the point where $q(z_0) = 0$. For the parameters shown in Figure 13 the curve $\Phi = (\pi/2 - Int)$ is almost coincident with the curve shown in Figure 14; the maximum difference is approximately 5%. In many other instances in which the WKB method definitely could not be applied we still have obtained relatively good agreement between the reflection coefficient phase given by the phase-integral technique and the phase given by the full-wave technique. Hence, in many instances we are allowed to determine the modes excited in a given duct by using only the function Φ. The results obtained in the following sections were derived by the

phase integral formula. However, the results were checked by the full-wave method at some important points.

Spectral behavior of the duct. Figure 16 gives the spectral behavior of one specific bell shaped duct. It gives Φ as a function of the angle of incidence for frequencies going from 1 to 9.5 kHz. The number by each curve is the corresponding frequency. All the curves begin at $\Phi = \pi/2$ for $I = 90°$ and end at the incident angle for which trapping fails. Observe that:

1. The mode $n = 0$ is crowded between $I \cong 75$ and 80° for frequencies above 1 kHz and for the specific parameters of Figure 16.

2. For a given mode n the upper cutoff frequency is the frequency for which the trapping process ceases before the phase of the reflection coefficient reaches $-n\pi$. For example, there is one upper cutoff frequency slightly lower than one-half of the gyrofrequency for the mode $n = 0$ (observe that, for $f = 9.5$ kHz, Φ does not reach zero).

3. There exists a lower cutoff frequency below which (53) is not satisfied; i.e., Φ is always positive, including at the

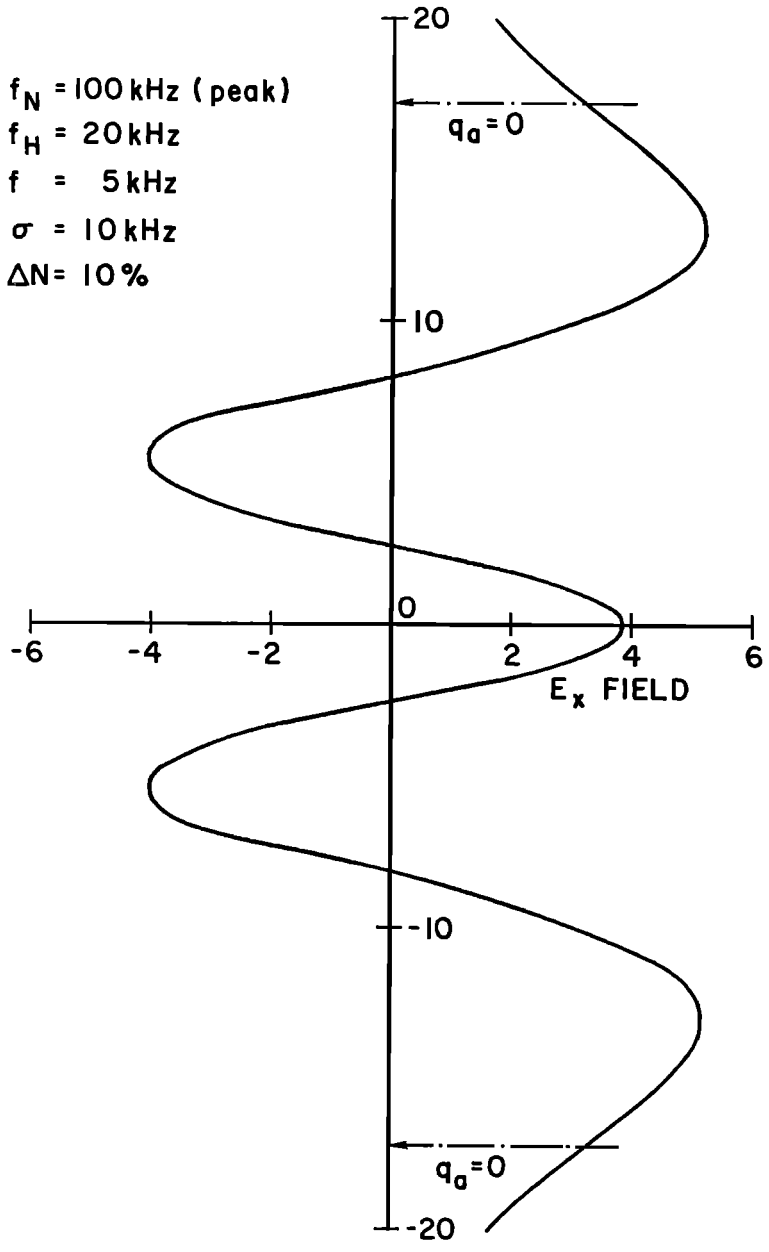

Fig. 15. Instantaneous x electric field for the mode $n = 4$. Same comments as for Figure 14. $I = 62°$ (from Figure 13).

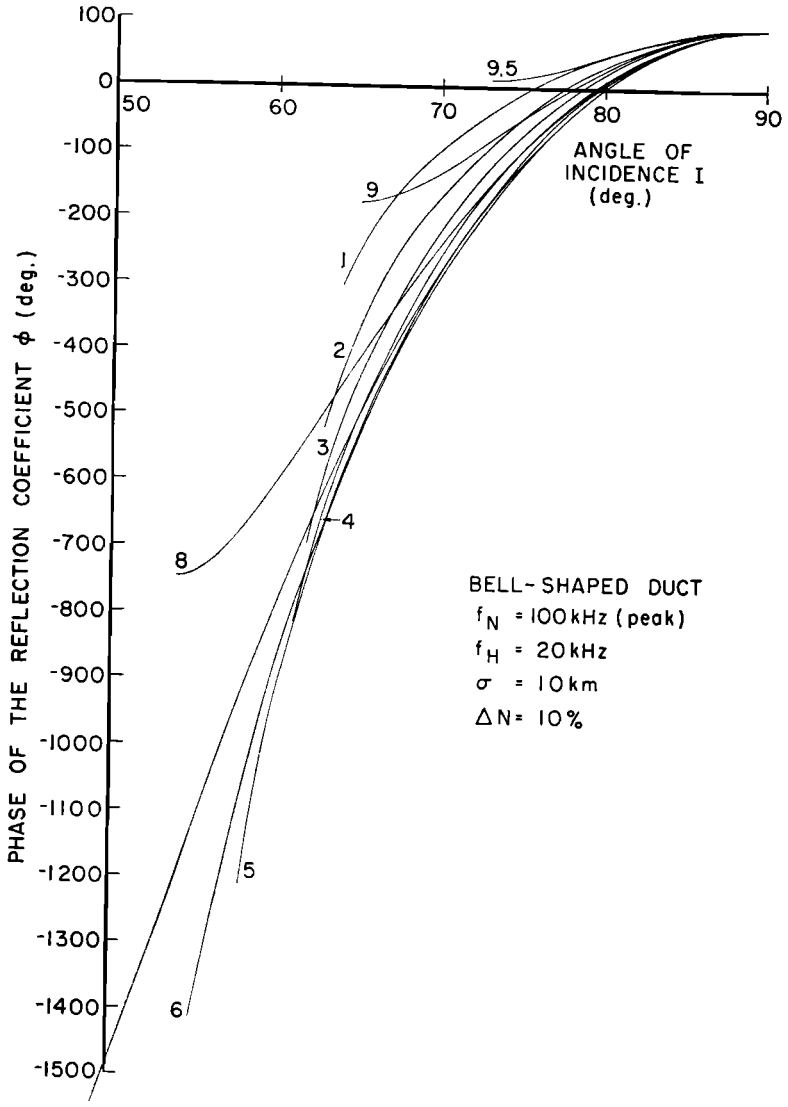

Fig. 16. Spectral behavior of a particular duct. The curves are parametric in frequency.

angle of incidence for which trapping is no longer achieved. This is not shown in Figure 16 but can be inferred from the behavior of curves for 3, 2, and 1 kHz in Figure 16. The lower cutoff frequency is highly dependent on the enhancement factor ΔN and on the thickness parameter σ.

4. The number of modes that can be excited for each frequency is small at low frequencies, increases, passes through one maximum (in our example, around 7 kHz), and decreases again going toward the cutoff frequency of the $n = 0$ mode.

Effect of changing the size of the duct. The effect of varying the size of the duct while the enhancement of ionization remains unchanged is shown in Figure 17. It is observed that when the duct is larger the number of excitable modes is also larger, as should be expected based on simple knowledge of metallic wave guides. The angle for which the waves are no longer trapped does not change because it depends only on ΔN and f.

Phase and group velocities. To satisfy Snell's law, the product $n_i S$ is a constant inside the duct for a certain angle of incidence at $z = 0$. Hence, the phase velocity inside the duct will be given by

$$v_p = c/n_i S \tag{57}$$

Thus, curves such as those shown in Figure 16 can be used for determination of the phase velocity of the modes. For each n the respective I is found; then (57) can be calculated.

The group velocity inside the duct can be approximately determined by using the phase integral formula. The group refractive index for a mode in the duct is

$$\mu_g = \frac{d}{df}(fn,S) = n,S + f\frac{d(n,S)}{df} \tag{58}$$

By using (56), *Walker* [1966*a*] showed that

$$\mu_g = (n,S) - \frac{\oint \left(q + f\frac{\partial q}{\partial f}\right) dz}{\oint \frac{\partial q}{\partial (n,S)} \cdot dz} \tag{59}$$

where the integral is taken around a closed contour in the z plane that encircles the branch points of q. This contour can be distorted to lie along the real axis by the choice of the correct branch of q. It can

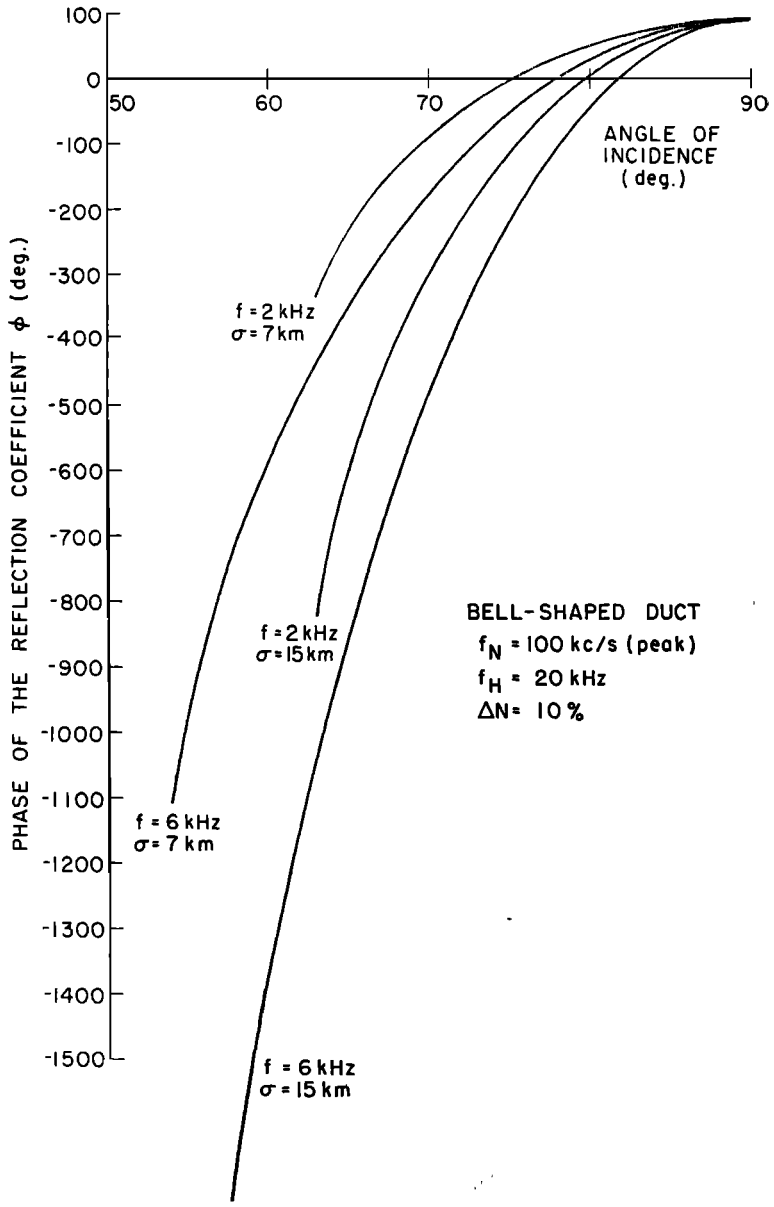

Fig. 17. Effect of varying the size of the duct without changing the enhancement of ionization. The curves are parametric in f and σ.

be put in the form

$$\mu_g = (n_i S) - \frac{\int_0^{z_0} \left(q + f\frac{\partial q}{\partial f}\right) dz}{\int_0^{z_0} \frac{\partial q}{\partial (n_i S)}\, dz} \tag{60}$$

where, again, z_0 is the point where $q(z_0) = 0$. Equation 60 is then calculated for each mode, that is, for each pair n, l. The group velocity comes from

$$v_g = c/\mu_g \tag{61}$$

Figure 18 shows the behavior of phase and group velocities for one specific duct. The phase velocity is given for the mode $n = 0$ and the group velocity curves are given for the lower modes $n = 0, 1, 2, 3$. The curve labeled L is the group velocity for a purely longitudinal wave that is propagating in the homogeneous medium whose ionization is the same as the peak of the duct. All curves have been calculated from $f = 1$ kHz up to the cutoff frequency. There are several important results from Figures 16 and 18:

1. In the low frequency band below the nose frequency ($\sim f_H/4$) the group velocities of all modes are the same. Observe that the number of modes is small for low frequencies, as shown in Figure 16.
2. For frequencies roughly above the nose frequency the group velocities of distinct modes are different. For higher modes the group velocity is smaller, as we could expect intuitively.
3. The cutoff frequency decreases for higher modes, as we could also expect from Figure 16 (see the curves for 9.5, 9, and 8 kHz).

7. SUMMARY AND CONCLUSIONS

In section 5 of this paper a full-wave computer method has been applied for studying VLF propagation in the magnetic meridian of a magnetosphere that is assumed to be locally planar stratified. More specifically, a study was made of the reflection and the transmission of waves through a half Gaussian variation of ionization such that actual magnetospheric irregularities could be simulated by varying an ionization parameter ΔN and a thickness parameter σ. The study of wave reflection that is based on the numerical full-wave technique and on the coupling theory showed that the principal cross-coupling parameters are very small for the sizes of the electron density irregularities usually found in the magnetosphere. On the other hand, the self coupling parameters are large only around a very narrow region that produces a reflected wave of the same kind as the incident wave. Therefore, the almost perfect reflection that occurs for a small difference in ionization between the two regions is understood in the light of

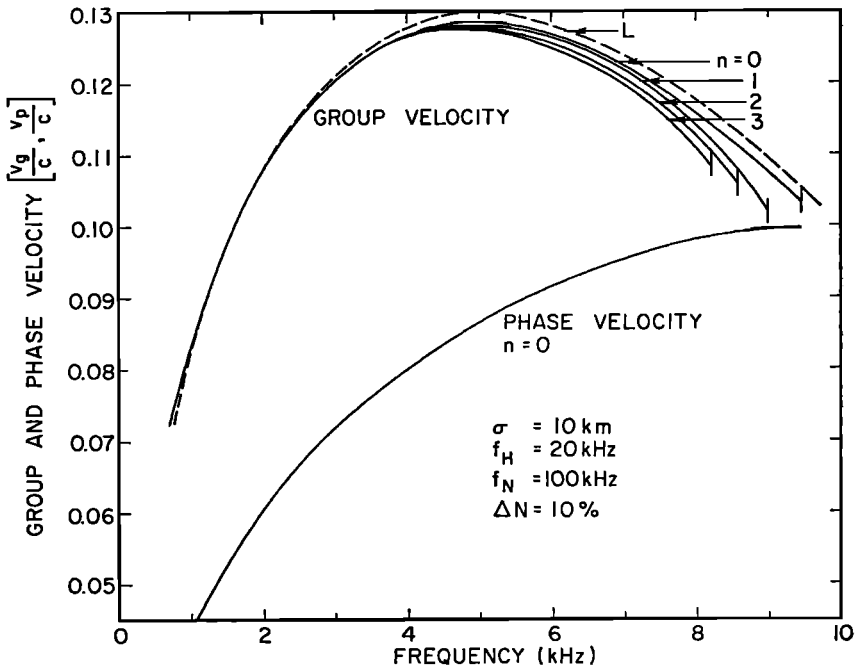

Fig. 18. Phase and group velocity as a function of frequency for several modes.

low cross-coupling between the incident wave a and the high-q b waves.

The studies of section 4 and 5 were extended in section 6 to include the mode theory of bell shaped ducts. The full-wave method provides wave-field structures across the ducts that resemble the solutions given by the Schrodinger equation for the wave functions of the harmonic oscillator. Comparisons between the full-wave method and the phase-integral method show that the phase-integral technique can be used for a wide range of medium parameters; the modal equation supplies very nearly accurate results compared with the phase of the wave fields given by the full-wave method.

There is an upper cutoff frequency for a given mode n such that above this frequency the trapping inside the duct ceases before the phase of the reflection coefficient at the symmetry axis of the duct reaches $-n\pi$. For the lowest mode $n = 0$ the upper cutoff is slightly below one half the gyrofrequency; this figure agrees with the ray-theory results of *Smith* [1961]. The upper cutoff frequency decreases as n increases. The mode theory also predicts a lower cutoff frequency; this prediction is based on the same physical reason for the upper cutoff; i.e. no trapping inside the duct before the phase of the reflection coefficient passes through zero. The lower cutoff frequency depends on the enhancement factor ΔN and on the width of the duct.

The wave-guide dispersion given by the mode theory differs from that in metallic guides, as shown by the frequency dependence of the phase velocity in Figure 18.

The excitation of a magnetospheric duct by a whistler packet corresponds to the excitation of an angular spectrum of wave normals inside the duct at each whistler frequency. The result will be the production of a large number of modes that will propagate independently from one hemisphere to the other. Figure 18 shows that under these conditions a very peculiar frequency-time spectrum of whistlers should be observed. This whistler would present several distinct traces at high frequencies; these traces should converge toward low frequencies. It is possible that this kind of mode whistler has been observed. However, a whistler of this kind would have the general appearance of a closely spaced multipath nose whistler train, and the present state of the theory does not give an unambiguous differentiation of the data. The mode theory developed here is limited to homogeneous ducts with N, ΔN, p, and f_H constants along the duct. Thus it is highly advisable to generalize the mode theory for variable ducts before comparing the mode predictions with whistler measurements. An important step toward the generalization of the mode theory has been taken in this paper by showing that the phase integral method can replace profitably the full-wave method in a variety of situations. The present mode theory for homogeneous bell shaped ducts can be extended to inhomogeneous ducts by generalization of the phase-integral method in a method similar to that proposed by Gothard [1968] but with the use of more realistic ionosphere models.

Acknowledgments. This research was supported in part by the National Aeronautics and Space Administration under grant NGL-05-020-008, in part by the Air Force Office of Scientific Research under grant AFOSR-783-67A,B, and in part by the National Science Foundation, Office of Computer Sciences, under grant NSF GP-948. The research was carried out under a graduate student research assistantship awarded to R. R. Scarabucci by Stanford University and a scholarship awarded by the Comissão Nacional de Atividades Espaciais, Brazil.

REFERENCES

Adachi, S. (1965), A study on the guiding mechanism of whistler radio waves, *Radio Sci. J. Res. NBS 69D*(4), 493–502.

Booker, H. G. (1962), Guidance of radio and hydromagnetic waves in the magnetosphere, *J. Geophys. Res.*, *67*(11), 4135–4162.

Budden, K. G. (1961), *Radio Waves in the Ionosphere*, first edition, Cambridge University Press, London.

Budden, K. G., and P. C. Clemmow (1957), Coupled forms of the differential equations governing radio propagation in the ionosphere, 2, *Proc. Cambridge Phil. Soc., 53* (P. 3), 669–682.

Clemmow, P. C., and J. Heading (1954), Coupled forms of the differential equations governing radio propagation in the ionosphere, *Proc. Cambridge Phil. Soc., 50,* 319–333.

Gothard, N. (1968), Guidance in the magnetosphere along field-aligned irregularities, *Radio Sci., 3* (3), 235–244.

Helliwell, R. A. (1956), Low frequency propagation studies, 1, Whistlers and related phenomena, *Final Rep. Contract AF19(604)795,* (June 15, 1953, to Sept. 30, 1956), Radio Propagation Lab., Stanford University, Stanford, California.

Helliwell, R. A., J. H. Crary, J. H. Pope, and R. L. Smith (1956), The nose-whistler—A new high latitude phenomenon, *J. Geophys. Res., 61*(3), 139–142.

Scarabucci, R. R. (1969), Analytical and numerical treatment of wave-propagation in the lower ionosphere, *Tech. Rep. SEL-69-046,* Radio Science Lab., Stanford University, Stanford, California.

Scarabucci, R. R., and R. L. Smith (1970), Full-wave treatment of wave-propagation through planar irregularities of

a magnetoionic medium, *Tech. Rep. SEL-70-046, Radioscience Lab.*, Stanford University, California.

Smith, R. L. (1961), Propagation characteristics of whistlers trapped in field-aligned columns of enhanced ionization, *J. Geophys. Res., 66*(11), 3699–3707.

Smith, R. L., R. A. Helliwell, and I. W. Yabroff (1960), A theory of trapping of whistlers in field-aligned columns of enhanced ionization, *J. Geophys. Res., 65*(3), 815–823.

Storey, L. R. O. (1953), An investigation of whistling atmospherics, *Phil. Trans. Roy. Soc. London, A, 246*, 113–141.

Voge, J. (1961), Propagation guidée le long d'un feuillet atmospherique our (plus particulièrement) exosphérique, Primière partie, *Ann. Telecomm., 17*(11/12) 288–295.

Voge, J. (1962), Propagation guidée le long d'un feuillet atmosphérique our (plus particulièrement) exosphérique, Deuxieme partie, *Ann. Telecomm., 17*(1/2), 34–43.

Walker, A. D. M. (1966*a*), The theory of the guiding of radio waves in the upper ionosphere, *J. Atmos. Terr. Phys., 28*, 747–767.

Walker, A. D. M. (1966*b*), The theory of guiding of radio waves in the exosphere, 1, Guiding of whistlers, *J. Atmos. Terr. Phys., 28*, 807–822.

Walker, A. D. M. (1966*c*), The theory of guiding of radio waves in the exosphere, 2, Waves propagating with small dispersion, *J. Atmos. Terr. Phys., 28*, 1039–1056.